2021-05-29

Morphological response of variable river discharge and wave forcing at a bar-built estuary

Orescanin, Mara M.; Coughlin, Jillian; Young, Walter R.

Elsevier

Orescanin, Mara M., Jillian Coughlin, and Walter R. Young. "Morphological response of variable river discharge and wave forcing at a bar-built estuary." Estuarine, Coastal and Shelf Science 258 (2021): 107438.
http://hdl.handle.net/10945/68919

Estuarine, Coastal and Shelf Science 258 (2021) 107438

Contents lists available at ScienceDirect

Estuarine, Coastal and Shelf Science

journal homepage: www.elsevier.com/locate/ecss

Morphological response of variable river discharge and wave forcing at a bar-built estuary

Mara M. Orescanin *, Jillian Coughlin, Walter R. Young

Naval Postgraduate School, Department of Oceanography, United States

ARTICLE INFO

Keywords:
Bar-built estuary
Beach breaching
Ephemeral river
Structure-from-Motion

ABSTRACT

Observations of morphological evolution at Carmel River State Beach, Carmel, CA, USA, were made during two winter periods where the estuary underwent transitions from closed to open states episodically during each observation period. However, each winter was climatologically distinct: the first (Dec 2016–May 2017) was a high river discharge year (several events >200 m^3/s) with westerly offshore waves and the second (Dec 2017–May 2018) was a low river discharge year with northwesterly offshore waves. The morphological response of the beach was measured using Structure-from-Motion from both aircraft and unmanned aerial vehicles (UAVs) and shows two distinct seasonal trends. The first (in 2016–2017) indicates rapid (hours) and frequent (days-weeks) migration of the river breach channel across the span of the beach. The second (in 2017–2018) indicates no migration of the initial breach channel, despite multiple breach events. Analysis of the offshore wave energy using the Coastal Data Information Program (CDIP) hindcast model results indicate a stronger longshore wave radiation stress during the migratory breach year. In addition, discharge rates during this year were more than three times stronger than the non-migratory year, indicating a stronger offshore jet from the breach site. These observations support the hypothesis that migration requires both a strong river discharge and a longshore wave radiation stress component.

1. Introduction

Some of the most dynamic and morphologically varying beach systems exist around beach breaching, such as those found at bar-built estuaries (or intermittently closed/open lagoons, ICOLs, McSweeney et al., 2017). Breaches create new openings along a beach that enable flow between two separate bodies of water (usually ocean and lagoon) and are challenging to quantify (both in hydrodynamics and in morphology) owing to rapidly changing field conditions (Kraus et al., 2002). Commonly, breaches reduce water levels within a lagoon or marshland, mitigating flooding in surrounding areas and allowing for the migration of marine life (Kraus et al., 2002; Orescanin and Scooler, 2018). Opening the backwater lagoon to waves from the bay or ocean facilitates exchange of water between the two water bodies and sometimes results in changes to the water quality (dominantly salinity) of the lagoon (Kraus et al., 2002).

Depending on the lagoon geometry and tidal prism, breaches can develop into tidal inlets, with a slower morphological evolution, common on barrier island systems (Aubrey and Speer, 1984; McSweeney et al., 2017) where there are three main processes causing inlet migration. These processes include 1. accretion of ebb tidal delta bars due to longshore sediment transport, 2. storm-induced shifts, and 3. ebb tide discharge around the inlet channel bend (Aubrey and Speer, 1984). Of these processes, only ebb tidal delta bar accretion occurs on a time scale of months, whereas the other two methods are observed to have a decadal reoccurrence or episodic (storm-based) effects (Aubrey and Speer, 1984).

In contrast to tidal inlets, there is little research regarding breach migration of ephemeral river mouths, or bar-built estuaries. Ephemeral rivers are characterized by varying flow intensity, largely driven by seasonal precipitation rates, and are common features globally, including along the North American west coast, Portugal, Australia, and South Africa. Ephemeral river mouths, similar to tidal inlets, can migrate, create new channels, and episodically breach through barriers (Behrens et al., 2009). In addition, circulation can be episodic owing to the presence of a sand sill at the river mouth (Williams and Stacey, 2016). Despite the common characteristic of intermittent seasonal precipitation, the breaching processes vary greatly even along the same

* Corresponding author.
E-mail addresses: msoresca@nps.edu (M.M. Orescanin), jcoughli@nps.edu (J. Coughlin), wryoung@nps.edu (W.R. Young).

https://doi.org/10.1016/j.ecss.2021.107438
Received 3 December 2020; Received in revised form 17 May 2021; Accepted 19 May 2021
Available online 29 May 2021
0272-7714/Published by Elsevier Ltd.

coast owing to changes in environmental forcing (wave exposure) and basin configuration, such that each system is unique (Clark and O'Connor, 2019).

Breaches at bar-built estuaries can occur both naturally and artificially (Kraus et al., 2002; Behrens et al., 2013). Natural breaches occur when high lagoon water levels cause scour through the beach or when seepage through porous sediment creates a lead channel (Pierce, 1970; Kraus et al., 2002; Kraus and Wamsley, 2003; Orescanin and Scooler, 2018). Alternatively, artificial breaches are created when channels are artificially dug across a beach barrier (Kraus et al., 2002; Orescanin et al., 2019). Artificial channels are generally created to reduce flooding in urban areas. These man-made channels can result in insufficient flow or early breach closure due to insufficient water build up to maintain the outlet (Kraus and Wamsley, 2003; Orescanin et al., 2019). Breach closures occur when consistently high tides and very high waves build up sand at the opening of an outlet (Pierce, 1970; Behrens et al., 2013; Orescanin and Scooler, 2018, Bertin et al., 2019) or by overtopping (Laudier et al., 2011). Furthermore, the shape of the outlet can determine the probability of breach closure: straight outlets have lower probability while curved outlets have higher probability owing to increased surface area and drag (Behrens et al., 2009; Orescanin and Scooler, 2018). Combining hydrodynamic parameters, specifically wave height and tides, limit closure events to occurring on the high tide with large waves (Behrens et al., 2013; Orescanin and Scooler, 2018), indicated when infragravity energy propagates into the lagoon (Orescanin and Scooler, 2018; Bertin et al., 2019).

In order to quantify the morphological evolution of a breaching beach system, it is necessary to topographically survey the system repeatedly, which can be difficult, time-consuming, and costly to conduct. Thus, not many studies evaluate bar-built estuary mouths, especially smaller ones (Carrivic et al., 2013). One key reason for this is lack of data on timescales appropriate for morphological evolution of these systems (hours to days). While terrestrial-based GPS surveys are possible, they are challenging and time consuming to complete at resolutions of interest for breaching and closure (sub 10m scale). Satellite observations may provide higher spatial resolution, but often lack the time resolution to observe individual breach and closure events. Structure-from-Motion (SfM) using unmanned aerial vehicles (UAVs) is a faster, cost-effective method of creating the required datasets for observing changes to elevation at specific locations (Westoby et al., 2012; Carrivick et al., 2013). Using overlapping photos taken at any angle, SfM estimates the camera position and meshes together similar terrain features in the photographs to create a point cloud of images (Snavely et al., 2008; Westoby et al., 2012). Ground control points (GCPs) are subsequently used to tie the point cloud into a coordinate system and create a dense point cloud (Westoby et al., 2012).

One bar-built estuary site, constrained by rocky headlands to the north and south, that exhibits variable seasonal and annual morphological evolution is Carmel River State Beach (CRSB), Carmel, CA, USA (Fig. 1, Fig. 11). Separating Carmel Bay from the Carmel River, CRSB seasonally breaches most years, causing morphological changes to the shape of the beach based on the initial location of the breach and the meanderings of the outlet after breaching (Kraus et al., 2002; Kraus and Munger, 2008; Orescanin and Scooler, 2018). The Carmel River breach is sheltered within Carmel Bay and is generally affected by offshore wave directions between 280 and 300° (James, 2005). Following the initial opening, the breach, historically will remain open 85% of the season prior to its final closure (James, 2005). The location of the breach was observed to form an elongated outflow to the north or south approximately 50% of the time between 1991 and 2005 (Example in Fig. 11, James, 2005). This elongation was hypothesized to be related to swell direction and overarching ocean conditions (James, 2005), but there has not been further research into this area. The other 50% of the time, the breach was straight (perpendicular) across the beach with no deflection to north or south. It should be noted that the observations that led to this statement were intermittent (not continuous).

Owing to the long-term (decadal) stability at Carmel River State Beach (Fig. 1c versus 1d), it is possible to study short-term (days to weeks) breaching events and smaller scale migrations (10s–100s of m) over many years without the need to consider larger scale migrations (100s of m to km), as might be seen at an unbounded beach with no rocky headlands. As seen in Fig. 1, this beach has historically maintained a similar width and length, despite the breaching by the Carmel River that occasionally results in migration of the river outlet on the scale of hundreds of meters, effectively altering the beach profile.

Past research into this system investigated the momentum balances between the lagoon discharge and ocean forcing, noting that breaches will occur during periods of increased discharge with constant ocean forcing and periods of constant discharge with decreased ocean forcing (Orescanin and Scooler, 2018). Additionally, Rich and Keller (2013) developed and performed model runs which demonstrated that breaches are generally controlled by discharge, or streamflow, and overtopping. Of these two mechanisms, overtopping driven breaches are usually "short-lived" when compared to streamflow driven events (Rich and

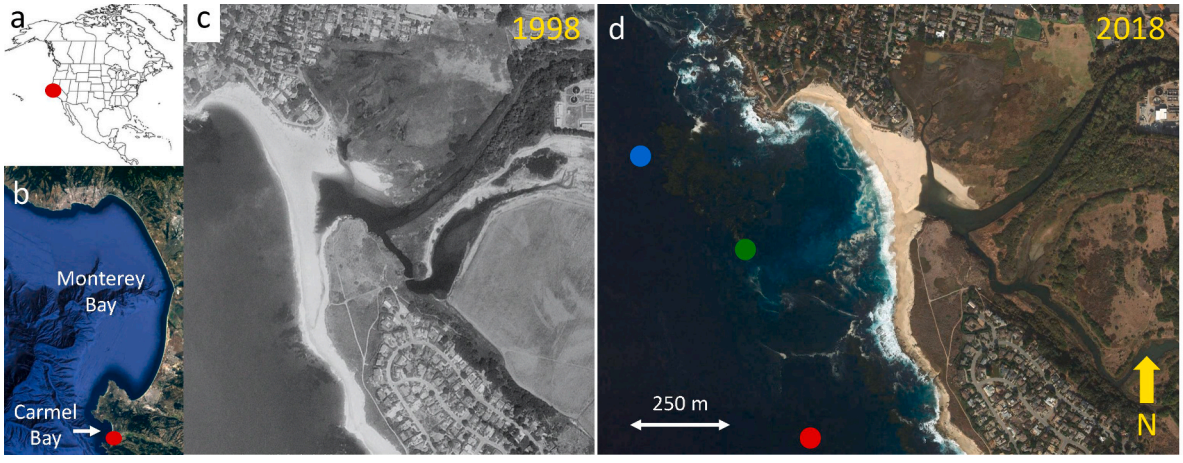

Fig. 1. Location of Carmel River State Beach (red circle) relative to a) North America and b) Carmel and Monterey Bays, CA. Carmel River State Beach from c) 1998 and d) 2018 at same scale. Red, green, and cyan circles in c) are CDIP MOP wave observation sites 630, 633, and 636, respectively. (For interpretation of the references to color in this figure legend, the reader is referred to the Web version of this article.)

Keller, 2013). Furthermore, the study found that decreased lagoon berm heights in the model allow for increased wave overtopping to occur while increasing the water elevation of the lagoon required to effectively breach the berm (Rich and Keller, 2013).

This study examines two subsequent breach seasons of the Carmel River: December 2016 to June 2017 and December 2017 to June 2018. During the first year, the breach initializes at the southern end of the beach, slowly migrates to the north from January to March, and then relaxes to the south for breach closure. This year saw higher rainfall than usual for the area. The following year (2017–2018), the breach formed at the southern end of the beach in early winter and remained in the same position for the duration of the breach season. Using aerial photography and the implementation of SfM photogrammetry and physical data (wave heights, wave direction, tides, water level, precipitation, and discharge rates), the existence of a pattern within the seasonal migration of the breach along the beach is proposed. The hypothesis of this study is that morphological stability could be balanced between years with and without river migration. Furthermore, it is hypothesized that migration of the Carmel River mouth is driven by river discharge (and berm height), but the phenomenon can be affected by large waves from storm events.

2. Materials and methods

Beach elevation surveys were conducted from December 2016 through September 2018 with aerial flights (by the United States Geological Survey (USGS)) and by an unmanned aerial vehicle (UAV) during various configurations of beach morphology (Table 1). These surveys span two seasons of barrier breaching and are used to determine the presence of morphological changes to the beach topography from month to month. All surveys required GPS-realized ground control points (GCPs) to tie the images to a reference coordinate system. This study used an Ashtech ProMark GPS receiver to record the location of GCPs after conducted flights.

2.1. Aerial surveys

The USGS team flew surveys of Carmel River State Beach using a Nikon D800 and a Nikon D810 mounted to a fixed-wing aircraft (Cessna 182) with a GPS antenna (aerial data published in Warrick et al., 2019). Both cameras operated at 36.3-megapixel resolutions and took pictures of the Carmel River State Beach at an oblique angle. The Nikon D800 camera used various focal lengths in flight (50 mm, 30 mm, and 40 mm) and the Nikon D810 used a focal length of 40 mm. These photographic surveys were conducted each month during the 2017 breach season (December 2016 through June 2017) and images had roughly an 85% overlap from a single pass flight. The following year, there were five additional surveys conducted (Table 1). The aircraft-produced images covered a large frame of view (km scale), including the surrounding roads and buildings, and each survey consisted of 37–52 images with an approximate horizontal resolution of 50 cm at the beach.

The USGS surveys did not use pre-positioned, study-specific GCPs. Therefore, fourteen GCPs (fixed features) were identified within the photographs and precise GPS of the GCPs was measured during fieldwork with the Ashtech ProMark. These GCPs consisted of high-contrast, easily identifiable features such as pothole covers, road markings, fence corners, signposts, and an elementary school foursquare court (Coughlin, 2018).

The root mean square error (RMSE) given in centimeters for the USGS GCPs is provided in Table 2. RMSE was calculated by retaining 1–3 GCPs closest to the beach that were not used to fit the aerial survey to the reference coordinate system. The coordinates of the unused GCPs could then be used to compare to the computed surface, resulting in the estimated error between SfM surface and unused GCP.

Table 1
Survey dates and breach locations. Bold indicates UAV survey, non-bold indicates USGS survey.

Survey Date	Breach Location
12/20/2016	South
01/25/2017	Central, dual outlets
02/22/2017	Central
August 03, 2017	North
May 04, 2017	South
05/19/2017	South
06/26/2017	South
June 12, 2017	**Closed**
12/21/2017	Closed
October 01, 2018	**South**
01/23/2018	**South**
01/29/2018	South
02/28/2018	**Closed**
July 03, 2018	South
05/17/2018	**South**
05/28/2018	South
October 09, 2018	Closed

2.2. UAV surveys

Either a DJI Phantom III Advanced quadcopter or a DJI Inspire I (with Zenmuse X3 camera), was flown over CRSB to conduct a survey of terrain elevation between the USGS flights. The collection dates (shown in Table 1) were targeted after channel migration and to augment the USGS survey dates. The UAV flight pattern was created with 70% side-to-side and 80% front-back image overlap in order to have sufficient feature overlap within the imagery. Each survey was flown at 60m elevation and yielded over 250 images with an approximate horizontal resolution of 5 cm.

Each survey date using the UAV had specific GCPs that were placed and measured during the flight. The GCPs used during the UAV surveys were 2.5-foot by 2.5-foot plywood boards painted with black and natural quad panels to allow for maximum contrast in aerial viewing. These GCPs were placed on the beach and in the immediate area and provide error estimates (Table 3) and were required because the survey area comprised mostly the beach and marsh that lacked permanent fixtures that could be used as routine GCPs, in contrast to the larger imaging area of the aerial surveys (which included surrounding roads, etc).

The root mean square error (RMSE) given in centimeters for the UAV GCPs is provided in Table 3. RMSE was calculated by retaining 1–3 GCPs closest to the center beach that were not used to fit the aerial survey to the reference coordinate system. The coordinates of the unused GCPs could then be used to compare to the computed surface, resulting in the estimated error between SfM surface and unused GCP.

2.3. Elevation surface creation

To measure the changes in elevation caused by sediment transport over time, a three-dimensional model of the beach elevation was created using SfM photogrammetry procedures for each survey flight. Overlapping photographs taken at various angles and embedded with GPS coordinates were input into the SfM software (Agisoft Photoscan Professional). SfM uses common features within the overlapping images to create “tie points” between all the images yielding a sparse point cloud. These aligned images are subsequently tied to a coordinate system, giving positioning and depth for pixel values, using a set of GCPs for each image set, and assigning XYZ values to the image pixels (Westoby et al., 2012). From here, a dense point cloud can be produced

Table 2
USGS GCP root mean square error: x-longitude, y-latitude, z-altitude.

Number of GCPs	X error (cm)	Y error (cm)	Z error (cm)	XY error (cm)	Total (cm)
12	33	37	16	50	53

Table 3
UAV GCP root mean square error: x-longitude/easting, y-latitude/northing, z-altitude.

Survey Date	Number of GCPs	X error (cm)	Y error (cm)	Z error (cm)	XY error (cm)	Total (cm)
June 12, 2017	5	2.8	3.3	23	4.3	23
October 01, 2018	4	2.5	4.8	4.0	5.5	6.8
01/23/2018	10	2.9	7.3	11	7.8	13
02/28/2018	9	1.1	2.5	29	3.1	29
05/17/2018	4	2.0	2.0	4.0	3.2	5.1

(maintaining the positioning data for the USGS and UAV survey flights) which results in the highest resolution point cloud extracted from the pixel values (Westoby et al., 2012). Dense point clouds must be quality controlled for erroneous values. These most notably result from images taken over water (notorious for changing optical properties and no fixed features) and any additional point with a z value outside two standard deviations of the surrounding area (de-spiking). For the morphological calculations here, these dense point clouds can be linearly interpolated onto a grid (1-m by 1-m).

In this study, the USGS data were processed without an initial lens calibration. However, the UAV images used an initial lens calibration using the standard Photoscan process. Image alignment used high accuracy and adaptive camera model fitting enabled for all survey dates. Additionally, the photographs were taken at significantly different angles specific to their platform. USGS images were taken at largely oblique angles and from significantly higher elevations (~400m) whereas all of the UAV data was shot top-down at low elevation (60m). The most noticeable result of this is spatial resolution (~5 cm for UAV surveys vs. ~50 cm for aerial surveys). One set of GCPs was used for all USGS survey dates. These GCPs canvassed the surrounding area and neighborhoods as the images from the aircraft covered a larger area. The GCPs were imported and individually placed for one survey date (May 19, 2017), saving two GCPs to use as check points. All USGS surveys were subsequently aligned to the May 19, 2017 survey to reduce human error introduced by individual GCP placement for each survey date.

Each UAV survey had date specific GCPs as the flight area was limited to the local beach area and GCPs had to be established on the beach itself via markers. These surveys were not aligned to one another. The SfM software built dense point clouds for every survey date. These datasets, once referenced by GCPs, are elevation maps of the observed area for each survey date. It is also recognized that for both aerial and UAV flights, measurements over the inland marsh (away from the barrier beach) may incur more error owing to distance from GCP locations and presence of dense vegetation. All errors reported are appropriate for the beach areas for all surveys.

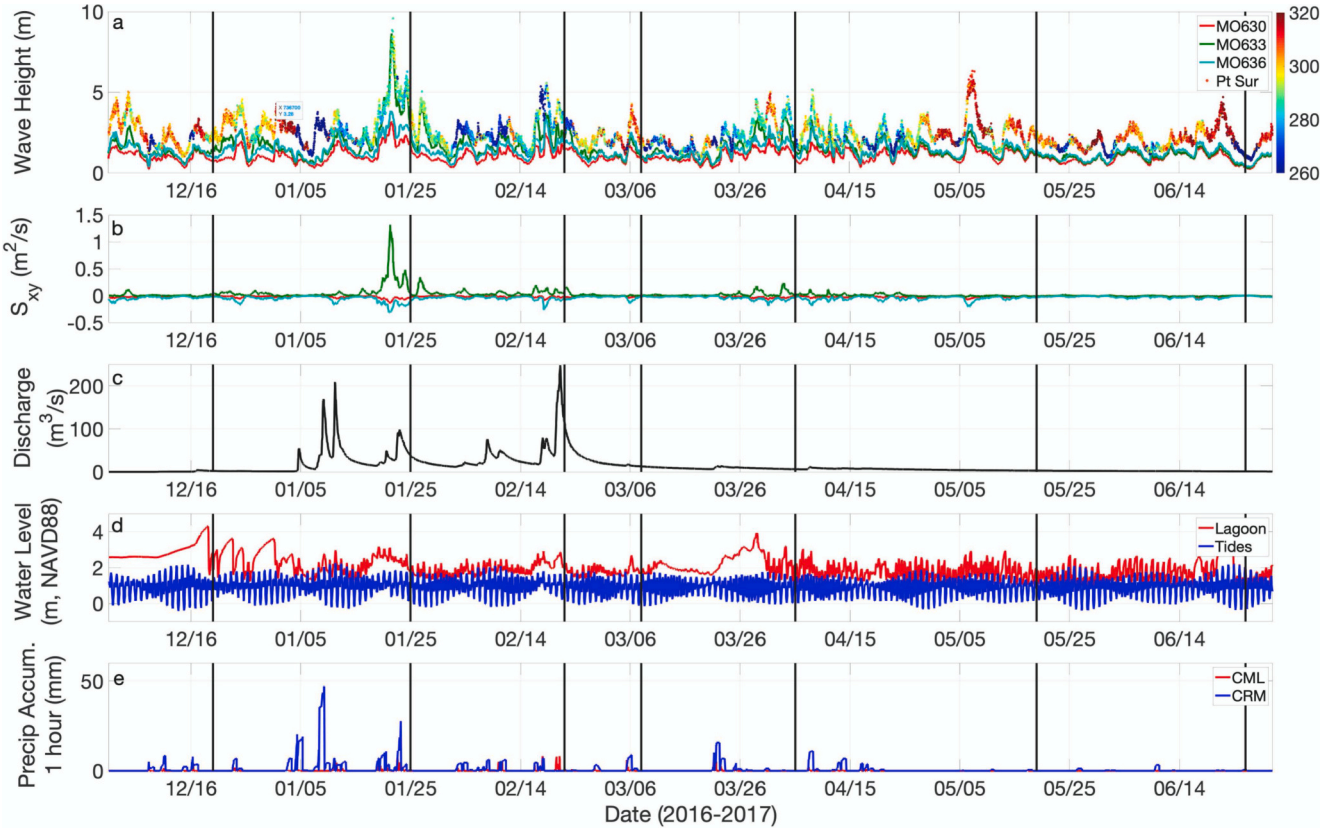

Fig. 2. Environmental time series during 2016–2017 winter where a) Wave height offshore (NDBC Pt Sur buoy) and onshore (CDIP MOP 630, 633, 636, Monterey County), b) resulting longshore (S_{xy}) wave radiation stress, positive is northward and colors same as in a), c) Carmel River discharge at the Hwy 1 bridge (from Monterey Peninsula Water Management District), d) water levels in the Ocean (tides at Cabrillo Point) and Lagoon (from Monterey Peninsula Water Management District), NAVD88, and e) precipitation accumulation (in mm) in Carmel Valley. Black vertical lines indicate timing for USGS flights. Gray shaded boxes denote timings of closure (no breach channel present). (For interpretation of the references to color in this figure legend, the reader is referred to the Web version of this article.)

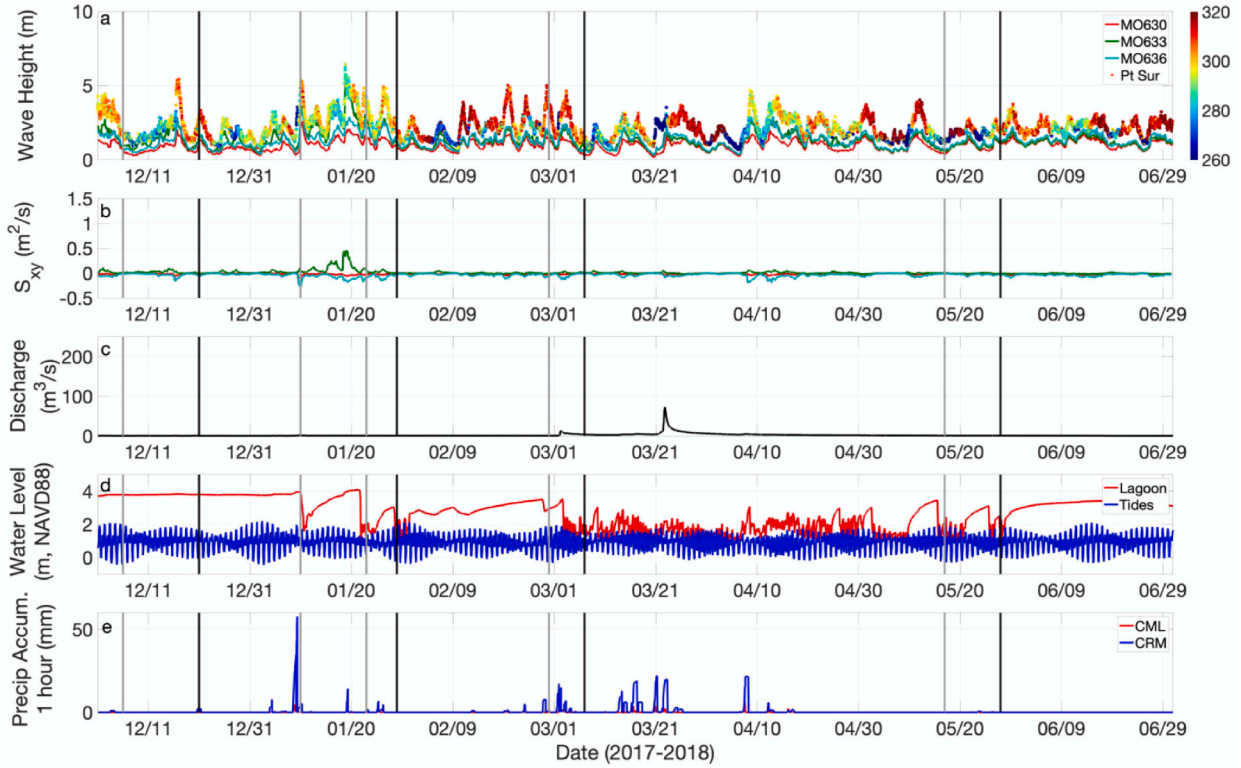

Fig. 3. Environmental time series during 2017–2018 winter where a) Wave height offshore (NDBC Pt Sur buoy) and onshore (CDIP MOP 630, 633, 636, Monterey County), b) resulting longshore (S_{xy}) wave radiation stress, positive is northward and colors same as in a), c) Carmel River discharge at the Hwy 1 bridge (from Monterey Peninsula Water Management District), d) water levels in the Ocean (tides at Cabrillo Point) and Lagoon (from Monterey Peninsula Water Management District), NAVD88, and e) precipitation accumulation (in mm) in Carmel Valley. Black vertical lines indicate timing for USGS flights and gray vertical lines indicate timing for UAV flights. Gray shaded boxes denote timings of closure (no breach channel present). (For interpretation of the references to color in this figure legend, the reader is referred to the Web version of this article.)

2.4. Wave heights and wave height gradients

Directional wave spectra measured every hour at the offshore National Data Buoy Center (NDBC) Station 46239 (Point Sur) are refracted shoreward to the 15-m isobaths approximately every 200 m alongshore in Carmel Bay at the Monitoring and Prediction sites (MOPs) as provided by Coastal Data Information Program (CDIP). The directional spectra at the MOP sites were integrated to obtain wave height (Figs. 2a and 3a) and radiation stress values (Figs. 2b and 3b). These datasets were verified and validated by the CDIP Program using MOP v1.1 validation dataset and Datawell's spectra layout with initialization parameters for both northern and southern California. The coordinates and locations of the three sites can be found in Fig. 1d. The datasets provide wave height, direction, period, and radiation stress from December 2016 through June 2018.

2.5. River and environmental datasets

River discharge (Figs. 2c and 3c) and lagoon water level (Figs. 2d and 3d) datasets were obtained from Monterey Peninsula Water Management District (MPWMD). River discharge was measured in cubic meters per second and lagoon water level was given in meters (NAVD88) every 15 min from December 2016 through June 2018. The discharge was measured at the HWY 1 bridge over the Carmel River.

Hourly tidal data (Figs. 2d and 3d) for Carmel Bay was collected from NOAA Tides and Currents Station 9413450 (Cabrillo Point), located at 36°36.3′N 121°53.3′W in Monterey Bay. This data provides the water level in meters, NAVD88.

Precipitation accumulation (Figs. 2e and 3e) was provided by the Citizen Weather Observing Program (CWOP) and California Irrigation Management Information System (CIMIS) at two weather stations in the Carmel area. Site 210 (CML) is located in Carmel Valley, CA, while EW6019 (CRM) is located in downtown Carmel-by-the-Sea, CA. Site 210 (CML) and EW6019 (CRM) sample rain accumulation every hour and every 15 min, respectively.

3. Results

3.1. External environmental forcing

The environmental factors during the two observed breach seasons are shown in Figs. 2 and 3. Data within these figures is a compilation of observations (NDBC wave heights, water levels, discharge, and precipitation), and CDIP model hindcasts (MOP wave heights, wave radiation stresses) that span upstream river conditions and offshore ocean conditions for a continuous two years.

3.1.1. The 2016–2017 breach season

From December 2016 to June 2017, the wave heights in Carmel Bay (estimated via CDIP MOP sites) were relatively consistent between one to 3 m with a few winter storm events exceeding 3 m (Fig. 2a). The wave heights from Point Sur were, on average, one to 3 m larger than the waves inside Carmel Bay. A maximum wave height of 10 m was observed at the end of January, between the first two survey dates (Table 1, vertical black lines Fig. 2). This observation is seen in the Point Sur data as well as at MOP633. The wave conditions are delayed in the CDIP plot due to propagation time from Point Sur to MOP633. Additionally, the data support that there is sheltering occurring at this location, largely due to the narrow aperture between Point Lobos and Carmel Point. There is a predominant wave direction at this location with the waves generally approaching from the west/northwest, varying in origin between 260 and 300°.

River discharge (Fig. 2c) are close to zero until the beginning of January when the discharge values begin to increase. The breach remained open for the majority of this observation season. Peak river discharge occurs in mid-February, increasing to 250 cubic meters per second. After this flow increase, the discharge levels begin to decrease and eventually cease as the river breach closes. In total, the season produced eight events with discharge rates above 50 m^3/s.

The lagoon water levels increased steadily until mid-December, peaking at 4.3 m prior to the initial natural river breach forming (Fig. 2d). Following this, the lagoon levels experienced a series of peaks as the breach stabilized itself, allowing water levels to increase in the lagoon prior to each subsequent breach (Orescanin and Scooler, 2018). For the remainder of the season, the lagoon levels fluctuated between one to 3 m elevation. Tides remain fairly constant throughout the season but are continuously at lower elevation than the lagoon water levels.

Finally, differences in precipitation along the coast (CRM) versus upstream in Carmel Valley (CML) show that generally more rainfall observed along the coast (Fig. 2e). Additionally, there is more frequent and higher accumulation precipitation events throughout January and February 2017.

3.1.2. The 2017–2018 breach season

Wave heights from December 2017 to June 2018 are not as varied as the previous breach season, with fewer winter storm events (Fig. 3a). The waves were consistently between one to 4 m high in Carmel Bay. The largest wave height for this season is about 6 m at the end of January, significantly lower than the previous year. The waves are observed to move in the same directions as the previous year. There is a slight increase in waves propagating from the northwest.

The river discharge levels (Fig. 3c) are very low with the maximum for the season occurring at the end of March with a discharge flow of 70 cubic meters per second. Compared with the 2016–2017 discharge levels and duration, this season only had one significant (>50 m^3/s) discharge event in contrast to the eight events of the previous season.

The lagoon levels (Fig. 3d) are relatively higher at the start of this season at approximately 3.75 m high, possibly owing to the low discharge flow rate. On January 9, 2018, the beach was artificially breached to avoid flooding in the local area surrounding the lagoon. The effect of this breach is observed as the first significant drop in the lagoon level. However, the artificial breach failed owing to lack of river discharge and the lagoon began to refill until the beach naturally breached approximately ten days later. Following this breach, the lagoon level oscillates throughout the remainder of the breach season until it begins to level off at the beginning of June.

Precipitation accumulation during this season (Fig. 3e) is similar to the previous season. Again, the coastal area received higher levels of rain. Differing from the previous season, this figure portrays increased rain events toward the end of the breach season in March and April 2018.

3.1.3. Wave height, direction, and wave radiation stress variability

Wave height differences between offshore and onshore waves (Figs. 2a and 3a) show fairly consistent differences throughout each breach season. The average difference between offshore and onshore waves is 1 m and is not dependent on offshore wave direction. The largest differences between the CDIP and Point Sur wave heights exist at the end of January during both seasons, during wave events with offshore wave heights above 4m. Throughout this period, the majority of the waves appear to come from due west instead of northwest.

To assess the transport direction of sediment, the longshore wave radiation stress estimates between a northern CDIP MOP site (MO636) and a southern CDIP MOP site (MO630) were compared (Figs. 2b and 3b). Wave radiation stress is the excess momentum flux owing to wave propagation. The cross-shore component (S_{xx}) describes the cross-shore flux of momentum. For this study, all S_{xx} values were found to be positive or onshore as to be expected with shoaling waves (not shown). S_{xy} describes the flux of longshore-directed momentum at the MOP sites. The positive values are in the northern direction while the negative values are in the southern direction. During both seasons, there are northerly radiation stress peaks. The first migratory season (2016–2017) experiences stronger S_{xy} values for a prolonged period of time whereas the second season (2017–2018) has lower S_{xy} signals (Figs. 2b and 3b). In fact, the first extreme northern migration of the breach channel occurred during the extreme wave event in January 2017, where S_{xy} values were a maximum. Using these results, longshore sediment transport is described using the Coastal Engineering Research Center (CERC) equation found in Orzech et al. (2010):

$$Q_{S,CERC} = KC_b S_{xy} \quad (1)$$

In this equation, $Q_{s,CERC}$ is longshore sediment transport, K is an (empirical) dimensional coefficient, and C_b is the phase speed of incident waves of at breaking. Since the only directional component in equation (1) comes from the radiation stress, the sediment transport is assumed to be proportional and oriented in the same direction (north/positive or south/negative).

3.2. Beach morphological evolution

Analysis of the photogrammetry surveys allowed for seasonal trends in morphology at CRSB from summer to winter to be established (summer – winter shown in Fig. 4) showing sediment loss during 2016–2017 and sediment gain during 2017–2018 to the barrier beach. Additionally, the differences between specific elevation maps were analyzed to observe the overall change in sediment movement, accretion or erosion, over the course of the breach season (Figs. 5 and 7), showing recovery of the beach after northward migration the previous year. Seven shore-normal beach cross-sections were positioned across the beach (Fig. 4b) to evaluate changes in beach elevation over time (Figs. 6 and 8).

3.2.1. The 2016–2017 breach season

From the 2016–2017 breach season surveys, the river outlet, or breach, migrated multiple times over the approximately 300 m stretch of the CRSB beach (Fig. 5) and resulted in a net loss of roughly 1.5m of elevation to the back beach area (Fig. 4a). The breach starts at the southern end of the beach (Fig. 5a) and migrates to the extreme northern end of the beach by the end of January (Fig. 5b) before returning to its original southern position in April (Fig. 5e). There were several observed northward migrations with the channel cutting across the southern spit of sand rapidly (within days) then migrating north (similar configuration to Fig. 5d). It was impossible to continuously survey but was noted from on-site images of sand scarps and channel location (not shown). After March, the breach channel remained to the southern part of the beach and the only variations in the channel were seen at the ocean most side (Fig. 5e–g).

The cross-section elevations (locations shown in Fig. 4b, cross sections in Fig. 6) in meters (NAVD88) for each survey date and allows for evaluation of the differences in elevation between the survey dates (i.e., how the beach is shifting). Starting in December 2016, a relatively constant beach crest elevation is seen throughout the cross-sections (from north to south, Fig. 6a and b) with the breach channel located toward the south (Fig. 6c). From December to January, there is an average beach elevation decrease of one to 3 m along the fore beach, assumed to be owing to winter wave events. The initial breach occurred on December 12, 2016, at the southern end of the beach. This breach episodically closed a few times until January 3 when it stabilized and would remain open for the remainder of the season (Fig. 2d). By January 25, 2017, the river breach had evolved and established two outlet channels located in the center of the beach. By February, accretion on the order of 2–4m occurred in the foreshore at the northern end of the beach (Fig. 6a and b) with accretion on the order of 1m occurring in the foreshore to the south (Fig. 6c). In March (Fig. 5d), the breach channel

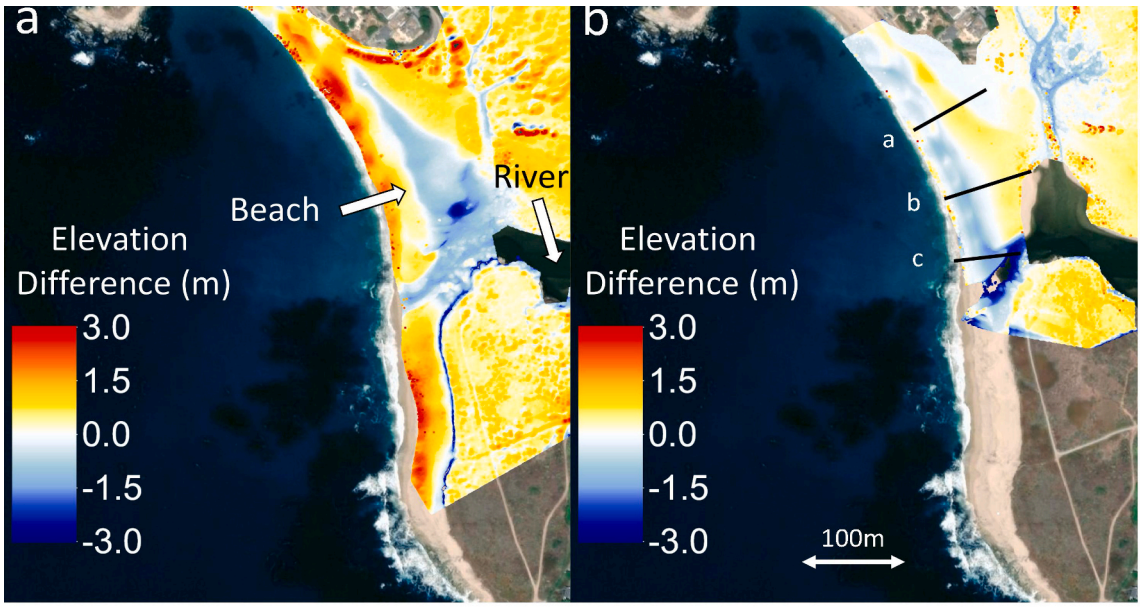

Fig. 4. Seasonal morphological change for a) June 2017–December 2016 and b) May 2018–December 2017 (summer/fall profiles were taken after/before all water year discharge events). Locations for cross section extraction labeled as black lines, a-c in b). Blank areas within the river indicate areas that were fully submerged, and therefore no measurements were made.

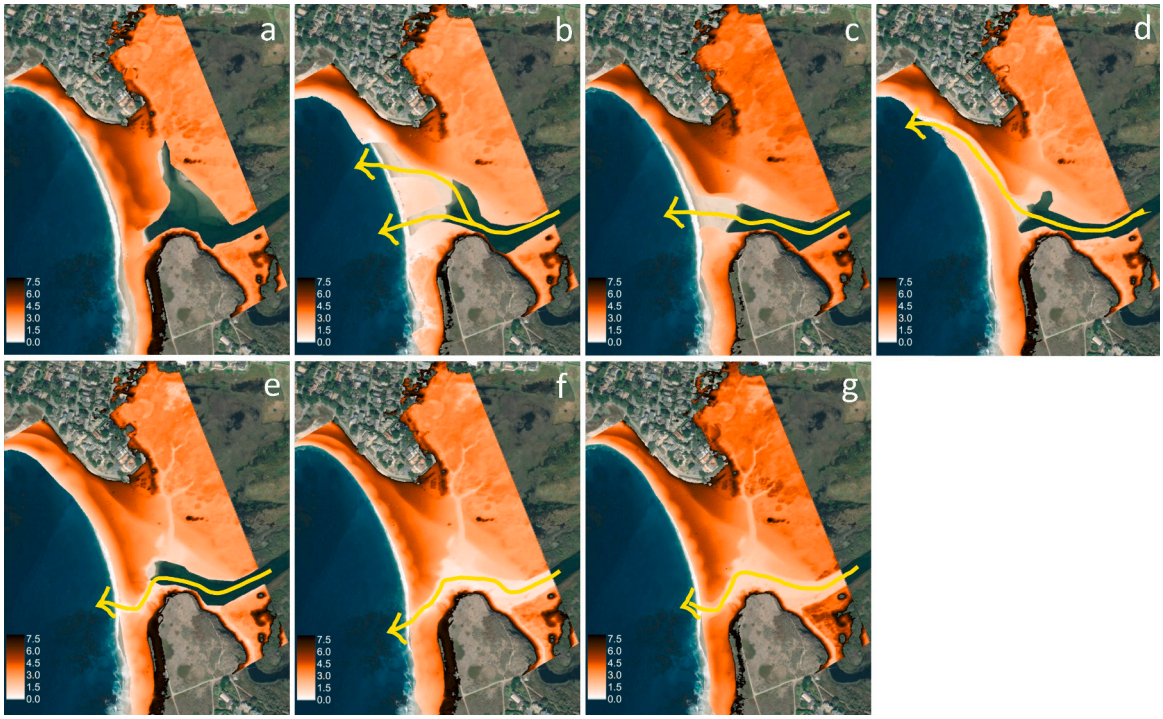

Fig. 5. Morphological evolution (2016–2017) for a) December 20, 2016; b) January 25, 2017; c) February 22, 2017; d) March 8, 2017; e) April 5, 2017; f) May 19, 2017; and g) June 26, 2017. Elevations provided for above water level in m, NAVD88. Errors provided in Table 2. All colored regions are areas exposed (sand) while any gaps in surveys were fully submerged (parts of the channel and/or lagoon). When the breach shifted along the beach, the data have been removed as the camera is unable to accurately distinguish depths through water. Yellow arrows indicate location of an active breach channel when present. (For interpretation of the references to color in this figure legend, the reader is referred to the Web version of this article.)

migrates approximately 190 m to the north where beach elevation is then observed to decrease by 4 m. However, by April (Fig. 5e), the breach has shifted back to the south and the northern beach elevations have rebuilt to 4 m high. May (Fig. 5f) and June (Fig. 5g) see minimal change in the beach elevation profiles aside from some beach building occurring at the southern foreshore as beach closure approaches. The breach was observed closed after July 14, 2017.

Throughout the entire breach season, the back beach from the center of the beach to the northern cross-sections (cross shore distance >100m Fig. 6a, >130m Fig. 6b) remains at a relatively constant level. This is

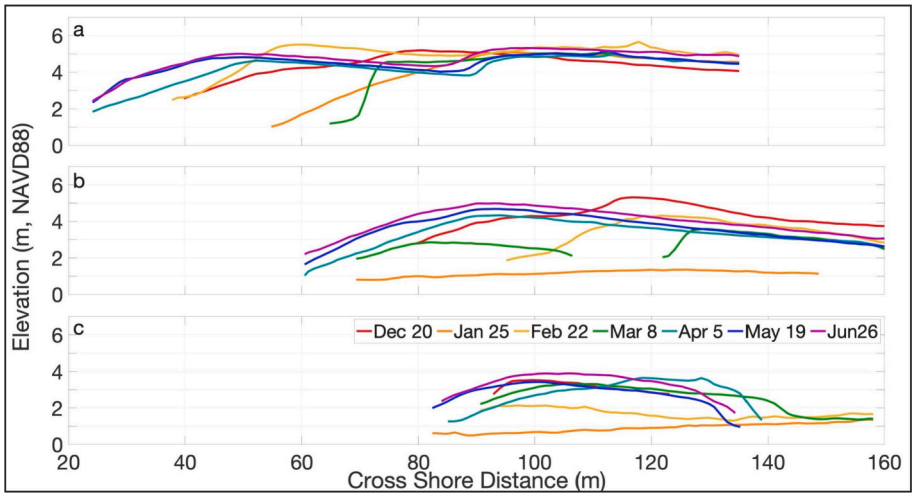

Fig. 6. Cross-sections (locations a-c in Fig. 4) from 2016 to 2017. All surveys shown are USGS aerial flights, with various breach locations (Table 1). Error is given in Table 2.

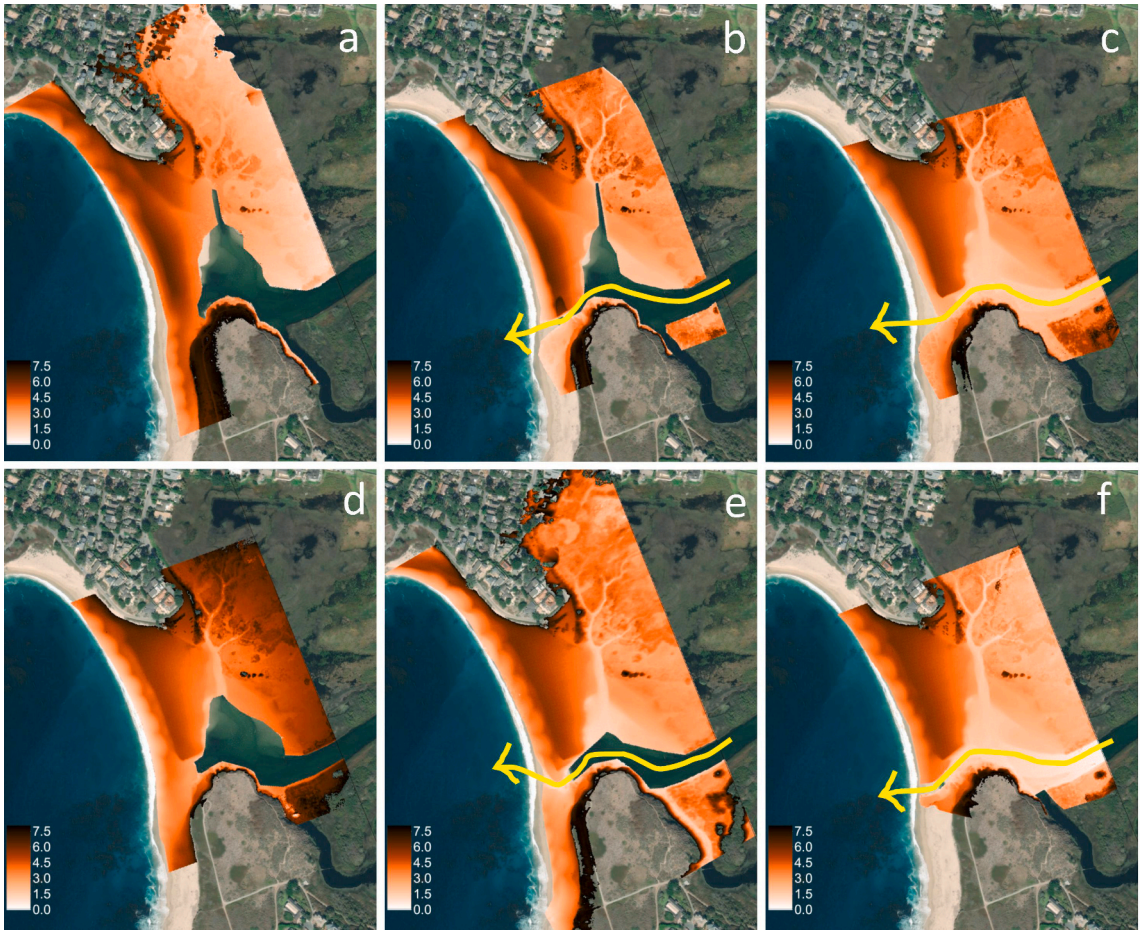

Fig. 7. Morphological evolution (2017–2018) for a) December 6, 2017; b) January 10, 2018; c) January 23, 2018; d) February 28, 2018; e) March 7, 2018; f) May 17, 2018. Elevations provided for above water level in m, NAVD88. Errors provided in Table 3. All colored regions are areas exposed (sand) while any gaps in surveys were fully submerged (parts of the channel and/or lagoon). When the breach shifted along the beach, the data have been removed as the camera is unable to accurately distinguish depths through water. Yellow arrows indicate location of an active breach channel when present. (For interpretation of the references to color in this figure legend, the reader is referred to the Web version of this article.)

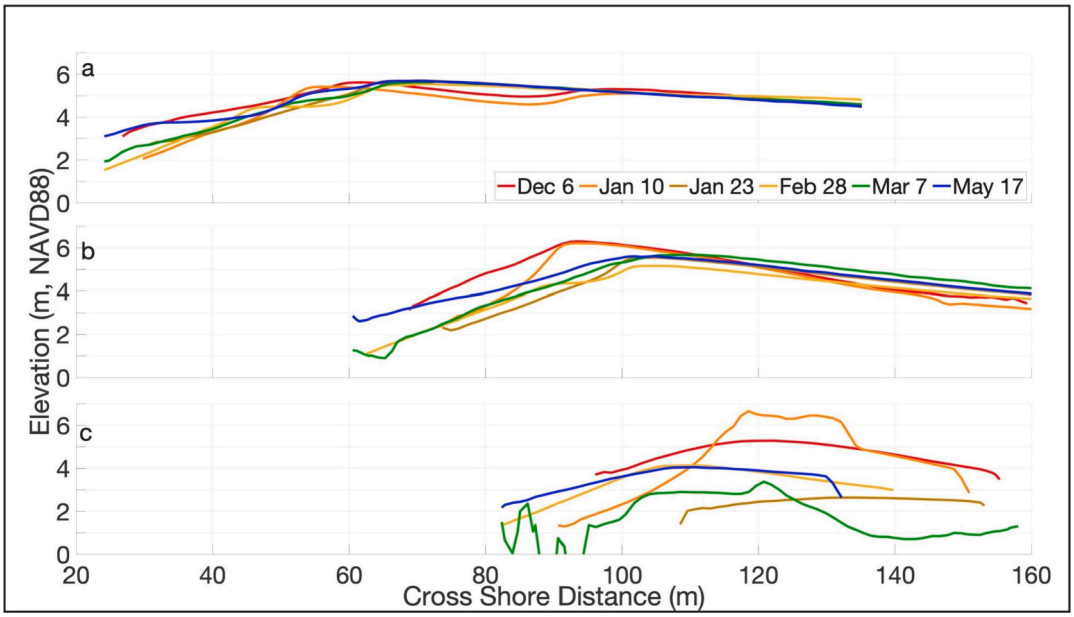

Fig. 8. Cross-sections (locations a-c in Fig. 4) from 2017 to 2018. All surveys except March 07 are UAV flights, March 07 is USGS. Other USGS flights not included for brevity. Breach locations described in Table 1, and error reported in Table 3.

where the higher beach berm resides. The back beach (cross shore distance between 70 and 90m, Fig. 6a and cross shore distance between 80 and 120m, 6b) sees an erosion of about 3 m in elevation throughout the season owing to the breach cutting through the beach. However, this area is beginning to be rebuilt by the end of the season (Fig. 6b and c, compare blue to purple).

3.2.2. *The 2017–2018 breach season*

In contrast to the previous season, the 2017–2018 breach season did not migrate from its initial breach location to the south (Fig. 7), and instead showed a net increase in beach elevation on the back beach (Fig. 4b). Consequently, the cross-sections for this season (Fig. 8) show less variation between survey dates. The initial breach of this season was an artificial breach conducted by Monterey County Resource Management Agency on January 9, 2018 (sand pile visible on the north side of the channel in Fig. 7b). However, the breach was not stable and closed within a few days. The first natural breach occurred on January 21, 2018.

From December (Fig. 7a) to early January (Fig. 7b), there is very little change across the beach, aside from the evolution of beach cusps. Between the early January (Fig. 7b) and February (Fig. 7c) survey flights, the back beach elevation increased by 1–2m at the middle and northern portions of the beach (also seen in Fig. 8a and b), erasing the outline of the northward migration from the previous season. Along the southern portion of the beach, additional areas of sand have been scoured down as the river cut through the beach (Fig. 7b–f, Fig. 8c). After these changes, the beach remains relatively the same shape until the May 17 survey. The breach was observed to be closed for the season after May 29, 2018 (Fig. 3d).

The beach elevations created via the UAV data agree with the elevations created using the USGS data (UAV and USGS shown in Fig. 8). However, through surveying at various dates, the UAV data provide a more detailed and higher-resolution examination of the 2017–2018 breach season and had lower error on average. This is especially seen in the back beach area (cross shore distance $>$ 100m, Fig. 8a and b) and is a result of GCPs located on the beach, yielding lower error. In Fig. 8a and b, the beach slope varies between survey dates and by the end of the season, the slope settles at a lower value than the start of the season, which is expected owing to smaller summer waves. The northern part of the back beach (cross shore distance between 60 and 100m, Fig. 8a) shows the infilling of the previous year's erosion noted in the seasonal morphological differences (Fig. 4). Furthermore, recovery of the southern part of the beach is also observed to the south (Fig. 8c).

Fig. 9. Schematic of dominant seasonal sediment transport trends with respect to channel migration for a) migratory years with net loss of sediment from the beach and b) non-migratory years with net gain of sediment to the beach. Blue arrows show possible locations of the river channel and orange arrows depict seasonal trends in sediment transport direction. Background imagery Google Earth (August 2017). (For interpretation of the references to color in this figure legend, the reader is referred to the Web version of this article.)

4. Discussion

4.1. Beach morphological evolution

The beach cross-section measurements show two distinctly different morphological trends for two environmentally different years that help explain the historical stability of CRSB (Fig. 9). During the 2016–2017 breach season (Figs. 5 and 6), the beach undergoes large (meter scale) elevation changes over the majority of the beach owing to river migration, ending the season with a net sediment loss to the back beach on the order of 2m (Fig. 4a). This is confirmed by repeated loss of sediment to nearly the entire beach area (regions in blue, Fig. 4a) as the channel migrates from south to north and back again (Figs. 5 and 6). By June, back beach levels have increased to about 3 m (NAVD88). However, the elevation does not return to the original height (pre migration, December 20, 2016), suggesting a net loss of sand from the back beach to the offshore (since elevations in the lagoon did not appreciably change either).

The following year, the beach profile in December is similar to how the previous season ended (compare June transects in Fig. 6 with December transects in Fig. 8), which indicates little morphological evolution during the intervening periods of small waves and no river discharge. From December to January, there is minimal variation in the elevation. This may be owing to the episodic openings and closings of the channel during this time (Table 1, Fig. 3). However, by March, the breach is stable and beach profiles display observable differences: to the south near the outlet location (Fig. 8c), river scouring removes sand from the beach resulting in a one to 2-m decrease in beach elevation at the 130-m cross-shore position. Conversely, on the back beach in Fig. 8a and b, sediment accretion (on the order of 1m) builds the beach and restores the back-beach elevation to its original height at the beginning of the previous season (December 2016, Fig. 6a and b)).

The RMSE for this study is on the order of tens of centimeters with the majority of the error occurring in the z-direction (Tables 2 and 3). Error for the USGS flights was slightly higher than the values observed for the UAV flights. This variation in error could be caused by the height

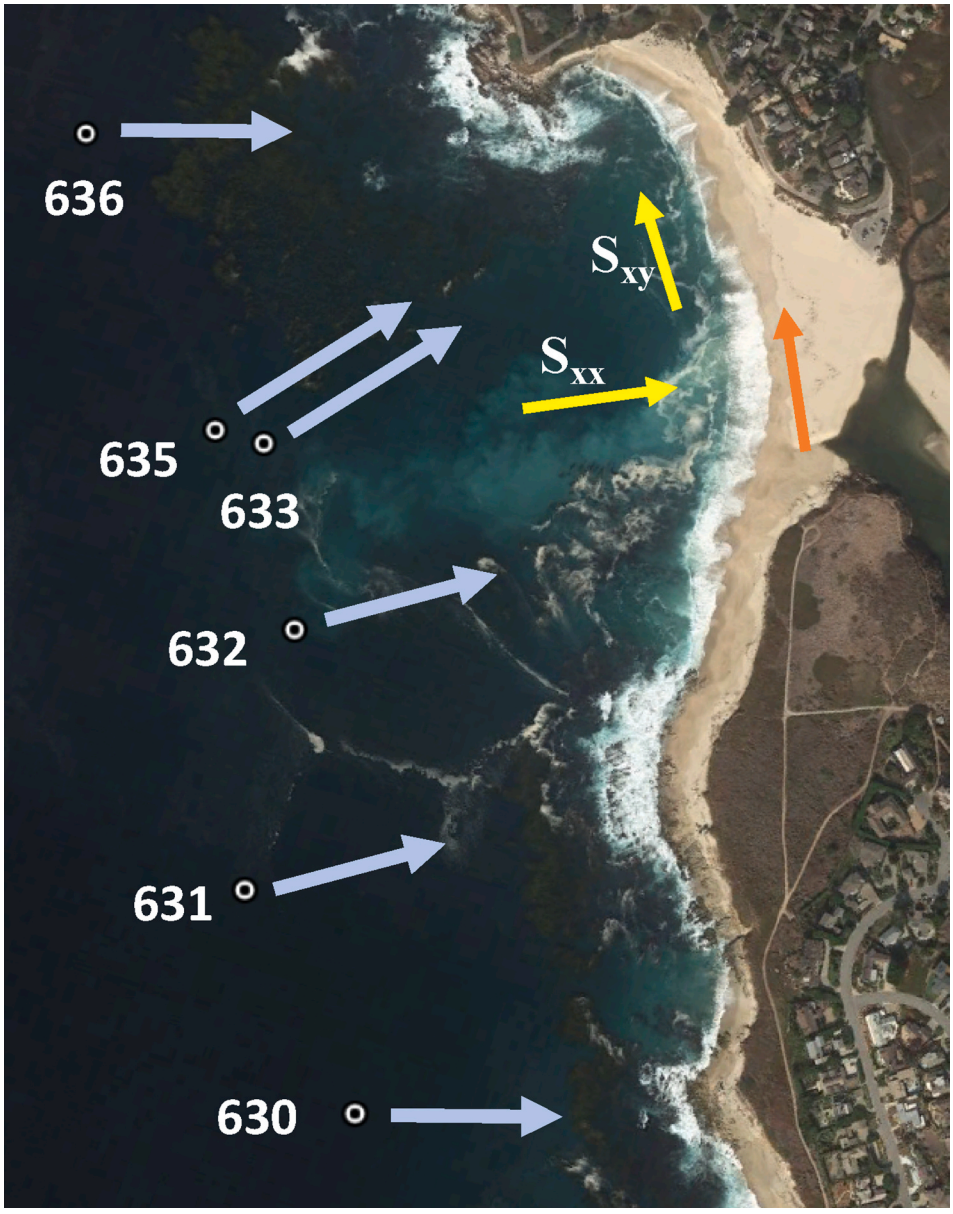

Fig. 10. CDIP MOP sites with average wave direction (blue arrows). Wave radiation stress directions indicated by yellow arrows. In the central part of the beach, onshore MOP 633, the longshore wave radiation stress would support transport in the north direction (orange arrow). Imagery from Google Earth. (For interpretation of the references to color in this figure legend, the reader is referred to the Web version of this article.)

of the flight path as well as the angle of the camera when the image was taken. However, these RMSE values are comparable to the 40–60 cm RMSE found by Rich and Keller (2013) at CRSB. The observed changes in beach morphology in this study are on the order of meters, thus the observed error will not have a major impact on the findings as the RMSE is an order of magnitude smaller. Total volume of migrated sediment was not calculated because integrating over a 10-cm error would induce huge errors in the calculation. Furthermore, with no bathymetry data, the sediment migration within the river outlet and offshore could not be accounted for.

These findings suggest the following statements regarding the long-term stability at CRSB: (1) during migratory breach years, the beach height and back beach extent decreases as it is scoured away by the outlet channel yielding net offshore transport (Fig. 9a); and (2) during stationary breach years, the beach begins to build back up where it had been eroded previously, yielding net onshore transport (Fig. 9b). From James (2005), fifty percent of the breach years at CRSB are migratory in nature. Given the historical stability shown in Fig. 1 and the observations of beach morphology, this study supports that a possible reason CRSB is a cyclical (or possibly) closed system for sediment transport is that patterns between migratory and stationary breach cycles lead to sediment loss from or sediment gain to the beach, respectively. Despite the headlands, which also support beach stability, if every year resulted in migrations similar to the 2016–2017 season, there could be retreat of the beach over time. It is not anticipated that progradation would happen in the opposite event of no migration as the beach height is limited by offshore wave climate and wave runup conditions.

It should be noted that the present study includes observations from only two years of morphological evolution. While these two years are climatologically distinct, especially in river discharge, it is not possible to conclude that similar years would have the same pattern of net sediment loss or net sediment gain. Instead, these observations can support the hypothesis that discharge is a critical variable for breach migration and that episodic migration could create a cyclic morphological trend at bar-built estuaries. Further morphological observations would be needed to support this cyclic hypothesis.

4.2. Wave-plume interaction

Wave direction from the 15m depth CDIP MOP sites display consistent directions throughout the two-year study period (time series are not shown for brevity, but the average wave direction shown in Fig. 10) while intensities vary with offshore wave climate (Figs. 2a and 3a). However, the direction varies by location from north to south, suggesting refraction within the basin, as expected. Both the extreme northern (636) and southern (630) MOP sites show consistent westerly waves (Fig. 10). The MOP sites between these two sites show slight variations in wave direction. MO631 and MO632 show waves from 255 to 260° while MO633 and MO635 show more southwesterly waves from 245°. These relative directions are plotted in Fig. 10 along with generic radiation stress (S_{xx} and S_{xy}), as discussed in Section 3.1.3.

In Fig. 2a, the extreme wave event in the end of January coincided with the first observation of northerly channel migration and large river discharge (>50 m^3/s). Furthermore, throughout the season, an observable shift in the offshore wave direction occurs from mid-January and through April 2017 (Fig. 2a) where the wave direction changes from northwesterly to predominantly westerly. This shift corresponds with periods when the river breach is open and continues to migrate from the south to the north of the beach (Table 1). These trends are marked by prolonged northward S_{xy} at MO633, which is the closest offshore location from the expected plume location suggesting a net transport of sand northward, that is larger from mid-January through April 2017 (Fig. 2b). Given the discharge levels were sufficient to prevent any closures during this period, it is expected that the river plume extended onto the inner shelf (outside the surfzone) where there were gradients in wave direction promoting northward deflection of the plume (Fig. 11). Evidence of foam lines suggest abrupt changes in water properties, consistent with the existence of an occasional offshore plume (Fig. 11a

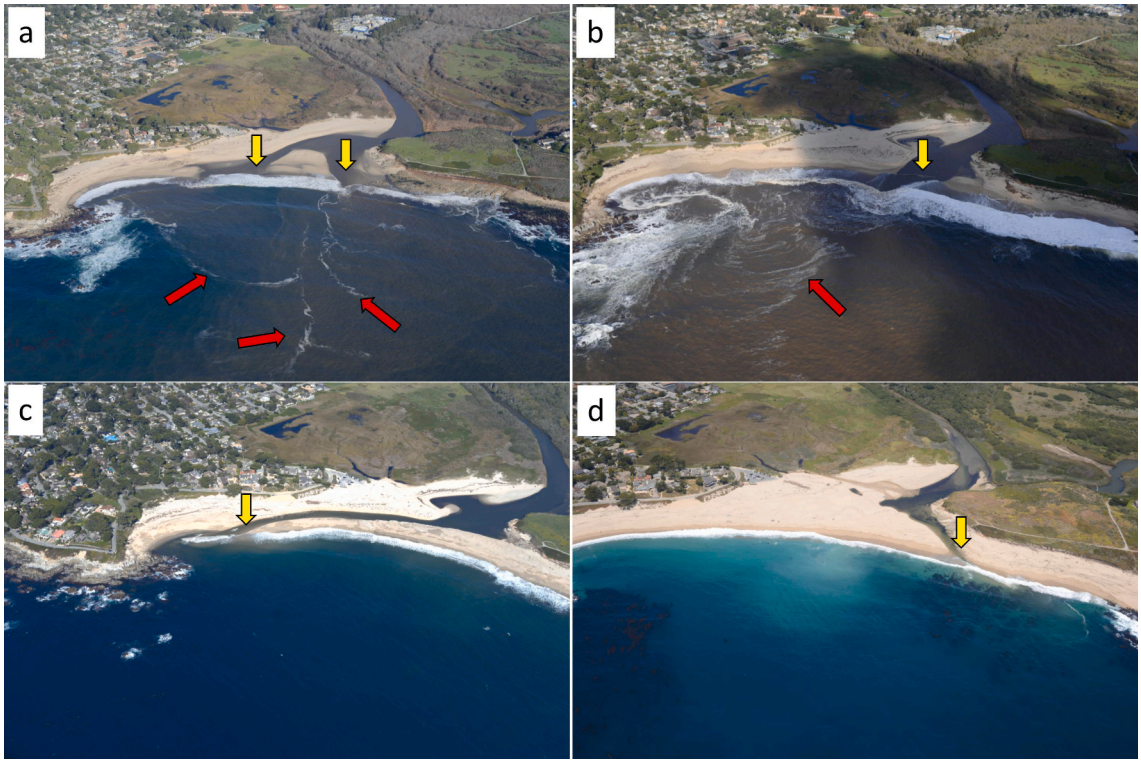

Fig. 11. Aerial imagery from USGS flights on a) January 25, 2017, b) February 22, 2017, c) March 8, 2017, and d) May 19, 2017. Yellow arrows indicate location of the breach entering the ocean while red arrows indicate foam lines (plume structure). Beach north-south distance (left to right in imagery) is approximately 500m. (For interpretation of the references to color in this figure legend, the reader is referred to the Web version of this article.)

and b). There are also several instances where discharge rates decrease, and no offshore foam lines exist, suggesting the plume is smaller or possibly mixed into the surfzone. Further studies should consider mapping locations of the river plume relative to the surfzone and river discharge in order to confirm this hypothesis.

Similarly, this wave direction pattern for 2017–2018 is similar to that in 2016–2017 (Figs. 2a, 3a and 10). In addition, there were several larger winter wave events (>5m H_s offshore, Fig. 3a), but in contrast to 2016–2017 (Fig. 2), there was weak river discharge (<2 m^3/s) in 2017–2018 (Fig. 3c), which lead to subsequent mouth closures from January through mid-March. While there is a similar seasonal shift in the offshore wave direction in 2017–2018 (Fig. 3a), the shift is not as prolonged as the first year (Fig. 2a) and the change in direction is not as pronounced. The waves shift from 300° to 280–290° and the shift only persists from late December through January (Fig. 3a) when the breach is often closed.

During the first season, there are higher river discharge rates (>50 m^3/s) for a continued period of time than during the second season (compare Figs. 2c and 3c). This high discharge occurs while the wave direction is shifted, and the river outlet is open and migrating to the north (Table 1). Conversely, the second season saw negligible river discharge leading to periods of prolonged closure until March, (Fig. 3c). The variation in river discharge from the first season to the second suggests that river discharge is one factor influencing migration of the channel.

The wave height gradient between offshore to onshore waves displays an average wave height difference of 1–1.5 m (Figs. 2a and 3a), supporting the sheltering that occurs within Carmel Bay. A longshore comparison of wave heights showed higher waves to the north of the beach in both breach seasons. During the first season, there is increased northern wave heights for a longer period of time corresponding with the period of westerly waves, high river discharge, and breach outlet migration to the north. However, despite the higher energy to the north, there is a greater northerly longshore component of wave radiation stress, suggesting orientation of incident waves is a second factor inducing northward migration. The second season also has higher waves to the north, but they are not sustained for a prolonged period, nor is discharge sufficiently high.

During periods of both seasons, the longshore radiation stress is to the north, and, therefore, northward migration of sediment is expected (Fig. 10). As longshore sediment transport is typically directly proportional to longshore radiation stress (S_{xy}), there is expected an increased northerly sediment transport occurring during the first season (Orzech et al., 2010). The result of this northward directed longshore radiation stress is that when the river plume is strong, it could cause northward deflection of the plume. This in turn could promote northward migration of the breach, as observed in the 2016–2017 season. The 2016–2017 season has both larger northward wave radiation stresses and significantly stronger discharge rates (compare ~50 m^3/s on average from January–April in 2017 to <5 m^3/s on average from January-mid March 2018) that both contribute to northward migration potential.

The fully 3D interaction between the breach plume, the surfzone, and the inner shelf wave gradients should be further investigated through numerical modeling and more-detailed offshore wave observations. However, the validation of the CDIP MOP sites, is well-established, providing initial support of the hypothesis that strong river discharge and northward wave radiation stress must co-exist for breach migration to occur.

In summary, the 2016–2017 breach season had heavier rain and higher river discharge than the 2017–2018 breach season. During the 2016–2017 breach season, there was northward directed wave radiation stress and sediment transport via longshore wave radiation stress (S_{xy}) created by the sustained offshore wave direction. The 2017–2018 breach season had less rain and thus minimal river discharge. The longshore wave momentum and sediment transport was reduced in comparison to the prior year. It is expected that higher discharge rates create stronger river plumes with greater offshore extent. While this is not explicitly observed at this site, it remains consistent that northward migration of the breach channel is observed during high river discharge (>10 m^3/s) with a northward component of longshore wave radiation stress. Given the existing dataset, it is not possible to determine whether there is a critical discharge required for migration and this remains an active area of research.

5. Conclusions

Two years of morphological observations at the Carmel River State Beach during two climatologically different breach seasons show seasonal variability in beach response. Owing to the migration of the breach, the morphological evolution of CRSB changes yearly. During a northward migration breach year (2016–2017), the beach experiences a loss of sediment on the back beach. However, during a no-migration breach year (2017–2018), the back beach gains sediment and accreted back to its pre-migration elevation. These findings suggest that there could be little net loss or gain of sediment to the system over a long period, promoting a closed or cyclical system for sediment transport.

This study concludes that the migration of the Carmel River breach outlet is influenced by both the wave climate and by the river discharge levels. Over the duration of this study, the wave climate at CRSB shows slight seasonal variations in wave direction, which caused enhanced northward directed wave radiation stress during the first year with prolonged wave direction from the west (rather than northwest). River discharge levels are critical in inducing the migration of the river outlet, by producing a strong offshore plume, where migration was observed during the high flow year and no migration was observed during the low flow year. Owing to the differences in river discharge between the two breach seasons in this study, an exact threshold required to induce migration was not established. Future study of seasons with moderate river discharge will be required to ascertain this value. This future work should also include the influence of mechanical versus natural breaching events on the overall morphology of the system. In addition, future studies would benefit from direct observation of wave heights to confirm the hindcast estimates from the CDIP MOPs at this site and offshore bathymetry to account for further changes offshore.

Bar-built estuarine mouth dynamics are a challenging area of study owing to the number of physical variables and difficulty in obtaining in-situ and rapid morphological and hydrodynamic observations. It should be noted, however, that such systems are all known to be influenced by both riverine and surfzone dynamics, namely river discharge and waves. The results of this study will therefore be helpful in addressing both the similarities and differences between different systems globally.

Author contributions

J. Coughlin was responsible for the majority of initial analysis as part of her master's thesis at the Naval Postgraduate School (June 2019). She collected the later 2018 data and developed the Structure-from-Motion methods for USGS flights with ground control points. W. Young collected the 2017–2018 UAS datasets and established the NPS Structure-from-Motion protocol for his master's thesis (June 2018). M. M. Orescanin was J. Coughlin's and W. Young's thesis advisor and supervised all data collection and analysis.

Funding

This research was supported by both the Naval Postgraduate School Naval Research Program and Office of Naval Research-CRUSER Program.

Declaration of competing interest

The authors declare that they have no known competing financial

interests or personal relationships that could have appeared to influence the work reported in this paper.

Acknowledgments

The authors would like to thank Jon Warrick and Andy Ritchie of the USGS for providing aerial imagery of the Carmel River, which was instrumental to this analysis. Thanks to Ed Thornton for providing feedback regarding this analysis. Thank you to Paul Jessen for field support and to Jeremy Metcalf for image processing support. Thanks to the Monterey Peninsula Water Management District for river discharge and water level data.

References

Aubrey, D.G., Speer, P.E., 1984. Updrift migration of tidal inlets. J. Geol. 92, 531–545.

Behrens, D.K., Bombardelli, F.A., Largier, J.L., Twohy, E., 2009. Characterization of time and spatial scales of a migrating rivermouth. Geophys. Res. Lett. 36 https://doi.org/10.1029/2008GL037025.

Behrens, D.K., Bombarelli, F.A., Largier, J.L., Twohy, E., 2013. Episodic closure of the tidal inlet at the mouth of the Russian river – a small bar-built estuary in California. Geomorphology 189, 66–80. https://doi.org/10.1016/j.geomorph.2013.01.017.

Bertin, X., Mendes, D., Martins, K., Fortunato, A.B., Lavaud, L., 2019. The closure of a shallow tidal inlet promoted by infragravity waves. Geophys. Res. Lett. 46 (12), 6804–6810.

Carrivick, J.L., Smith, M.W., Quincey, D.J., Carver, S.J., 2013. Developments in budget remote sensing for the geosciences. Geol. Today 29, 138–143. https://doi.org/10.1111/gto.12015.

Clark, R., O'Connor, K., 2019. A systematic survey of bar-built estuaries along the California coast. Estuarine. Coast. Shelf Sci. 226, 106285.

Coughlin, J., 2018. Morphology changes to Carmel River State Beach in relation to waves and river discharge. NPS thesis. https://calhoun.nps.edu/handle/10945/62839.

James, G.W., 2005. Surface Water Dynamics at the Carmel River Lagoon Water Years 1991 through 2005. Monterey Peninsula Water Management Agency, Monterey, CA.

Kraus, N.C., Militello, A., Todoroff, G., 2002. Barrier breaching processes and barrier spit breach, stone lagoon, California. Shore Beach 70, 1–22.

Kraus, N.C., Wamsley, T.C., 2003. Coastal Barrier Breaching, Part 1: Overview of Breaching Processes. Coastal and Hydraulics Engineering Technical Note ERDC/CHL CHETN-IV-56. U.S. Army Engineer Research and Development Center, Vicksburg, MS.

Kraus, N.C., Munger, S., 2008. Barrier beach breaching from the lagoon side, with reference to northern California. Shore Beach 76, 33–43.

Laudier, N.A., Thornton, E.B., MacMahan, J., 2011. Measured and modeled wave overtopping on a natural beach. Coast Eng. 58 (9), 815–825.

McSweeney, S.L., Kennedy, D.M., Rutherfurd, I.D., Stout, J.C., 2017. Intermittently closed/open lakes and lagoons: their global distribution and boundary conditions. Geomorphology 292, 142–152.

Orescanin, M.M., Scooler, J., 2018. Observations of episodic breaching and closure at an ephemeral river. Continent. Shelf Res. 166, 77–82.

Orescanin, M.M., Young, W., Coughlin, J., Herrmann, D.W., Metcalf, J., 2019. Seasonal Morphological Change at a Bar Built Estuary: Carmel River, CA. Coastal Sediments '19 World Scientific.

Orzech, M.D., Thornton, E.B., MacMahan, J.H., O'Reilly, W.C., Stanton, T.P., 2010. Alongshore rip channel migration and sediment transport. Mar. Geol. 271, 278–291. https://doi.org/10.1016/j.margeo.2010.02.022.

Pierce, J.W., 1970. Tidal inlets and washover fans. J. Geol. 78, 230–234.

Rich, A., Keller, E.A., 2013. A hydrologic and geomorphic model of estuary breaching and closure. Geomorphology 191, 64–74.

Snavely, N., Seitz, S.M., Szeliski, R., 2008. Modeling the world from internet photo collections. Int. J. Comput. Vis. 80, 189–210. https://doi.org/10.1007/s11263-007-0107-3.

Warrick, J.A., Ritchie, A.C., Schmidt, K.M., Reid, M.E., Logan, J., 2019. Characterizing the catastrophic 2017 mud creek landslide, California, using repeat structure-from-motion (SfM) photogrammetry. Landslides 16 (6), 1201–1219.

Westoby, M.J., Brasington, J., Glasser, N.F., Hambrey, M.J., Reynolds, J.M., 2012. 'Structure-from-Motion' photogrammetry: a low-cost, effective tool for geoscience applications. Geomorphology 179, 300–314. https://doi.org/10.1016/j.geomorph.2012.08.021.

Williams, M.E., Stacey, M.T., 2016. Tidally discontinuous ocean forcing in bar-built estuaries: the interaction of tides, infragravity motions, and frictional control. J. Geophys. Res.: Oceans 121 (1), 571–585.